Optimization of the Epilayer Design for the Fabrication of Doped GaN Planar Gunn Diodes

S. García-Sánchez, I. Íñiguez-de-la-Torre, S. Pérez, T. González, *Senior Member, IEEE*, and J. Mateos, *Member, IEEE*

***Abstract*— By means of Monte Carlo simulations of gallium nitride (GaN) planar Gunn diodes, the epilayer structure on which they are fabricated is optimized in order to achieve ultrahigh-frequency oscillations. Practical considerations, such as the limitations of the technological fabrication process and the mitigation of the huge self-heating effects expected to appear in the devices, have been also contemplated for the choice of the optimal epilayer parameters. The best results are obtained for an active layer thickness of 150 nm with doping of 5×10^{18} cm^{-3}, which would provide 350 GHz Gunn oscillations when using a contact separation of 0.5 μm.**

***Index Terms*— Doped gallium nitride (GaN), Gunn diodes, Monte Carlo simulations, terahertz (THz) generation.**

I. Introduction

TERAHERTZ (THz) wavelengths are of great interest for different applications in diverse fields such as medical imaging, biology, security, telecommunications, pharmacy, sensors, quality control mechanisms, or in the aerospace industry [1], [2]. Although a huge research work is being made both from electronics and optics approaches to explore the so-called THz gap, there is still much road to travel in order to make these applications broadly accessible. Indeed, photonic systems are usually bulky and difficult to operate, and devices as quantum cascade lasers [3] are incompatible with many consumer applications because they are operational only at cryogenic temperatures. Therefore, electronic devices seem to be the most practical way for the development of room-temperature, compact, and low-cost THz applications. In order to achieve signals in the THz region, different electronic sources based on semiconductor devices have been studied: from frequency multipliers based on Schottky diodes [4]–[6] to monolithic microwave integrated circuits (MMICs) based on transistors [7], [8] and active two-terminal devices like resonant-tunneling diodes [9]–[11], transit-time diodes (impact ionization avalanche transit-time (IMPATT) [12], [13] and tunnel-injection transit-time (TUNNETT) [14]–[16]), or transferred-electron devices (also called Gunn diodes [17], [18]) which generate output power taking advantage of a negative differential resistance (NDR) at the frequency of interest. In particular, the simple, compact, and flexible planar Gunn diode (PGD) architecture is gaining popularity in the last years, GaAs- and InGaAs-based PGDs have demonstrated fundamental oscillation frequencies of 120 GHz (the highest for a GaAs-based Gunn diode [19]) and above 300 GHz [20], respectively.

The development of gallium nitride (GaN) technology has made significant inroads into high-power and high-frequency applications with respect to other semiconductors and has emerged as one of the most promising materials for high-power applications at microwave frequencies [21]–[24]. Interestingly, even if no functional GaN Gunn diode has been realized up to now, simulations predict the appearance of Gunn oscillations (GOs) in GaN diodes [25]–[32]. On the other hand, indirect evidence of current oscillations in GaN diodes [33], [34], together with the recent observation of NDR in GaN vertical diodes [35], [36], allow us to envisage the practical feasibility of high-power high-frequency GaN Gunn diodes.

GaN PGDs based on the geometrical shaping approach [37] are promising candidates to achieve efficient GOs, as we have shown in previous works [31], [38] [see Fig. 1(a)]. Efforts are being devoted to the fabrication of such shaped GaN PGDs including an important novelty: the use a doped GaN active layer instead of the typical AlGaN/GaN epilayers employed so far. Indeed, some epilayers based on doped GaN have already been grown [39], [40] and devices will be soon fabricated.

In the case of the AlGaN/GaN heterostructures, the space charge created by the Gunn domains is associated with the positive surface charge located at the heterojunction, developing within an undoped GaN layer, so that it cannot change abruptly. In contrast, by increasing the doping of the active layer, the Debye length is much reduced, so that the formation of the Gunn domain is promoted by the presence of a higher

Manuscript received July 30, 2021; revised October 21, 2021 and December 1, 2021; accepted December 9, 2021. Date of publication December 23, 2021; date of current version January 24, 2022. This work was supported in part by the GaNGUN Project under Grant NRF2017-NRF- ANR003, in part by the Spanish Ministerio de Economía y Empresa (MINECO) and Fondo Europeo de Desarrollo Regional (FEDER) under Project TEC2017-83910-R, and in part by the Junta de Castilla y León and FEDER under Project SA254P18. The review of this article was arranged by Editor S. Chowdhury. *(Corresponding author: S. García-Sánchez.)*

S. García-Sánchez is with the Departamento de Physics and Mathematics, University of Alcalá de Henares, 28801 Madrid, Spain (e-mail: sergio.garcias@uah.es).

I. Íñiguez-de-la-Torre, S. Pérez, T. González, and J. Mateos are with the Applied Physics Department and USAL-NANOLAB, University of Salamanca, 37008 Salamanca, Spain.

Color versions of one or more figures in this article are available at https://doi.org/10.1109/TED.2021.3134927.

Digital Object Identifier 10.1109/TED.2021.3134927

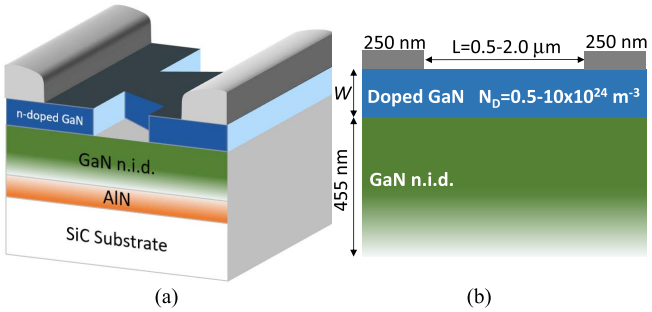

Fig. 1. (a) 3-D geometry of the shaped Gunn diodes. (b) Simulated epilayer structure.

electric field which appears very fast in the close vicinity of a space charge outbreak. Therefore, the main benefit of the use of a doped GaN active layer is the enhanced strength of the local electric field when a charge imbalance appears, with the additional benefit that it can be modulated by means of the doping level. Then, the first step in the optimum design of shaped diodes is the choice of the most adequate epilayer structure. For this sake, in this article, we report on detailed Monte Carlo simulations of GaN PGDs. We take into account not only the ideal simulation results with careful consideration of surface effects but also the constraints imposed by the technological process for the fabrication of the devices and its practical implementation (mainly to avoid excessive self-heating in continuous-wave operation). For this sake, we will perform simulations of (unshaped) PGDs using active layers with different doping and thickness with the aim of increasing as much as possible the frequency and power of the GOs.

II. Device Details and Monte Carlo Simulations

With the aim of providing the design rules for the fabrication of GaN-based Gunn diodes in shaped planar nanodiodes [41], such as the tapered-channel diode shown in Fig. 1(a) as an example, we have simulated just the simple epilayer structure sketched in Fig. 1(b). The design of V-shaped channels defined by thin trenches proposed in [31] has been slightly modified to focus on the tapered channels shown in Fig. 1(a) for two reasons: 1) technological difficulty, since narrow trenches are hard to define when a thick active layer is used and 2) physical effect, since the surface charges at the outside wall of the trenches may enhance the depletion of the channel, thus acting against the formation of the Gunn domains.

The doping, N_D, and thickness, W, of the doped GaN layer will be treated as optimization parameters in order to improve the figures of merit of fabricated GaN PGDs. The features of the GOs obtained in such simple PGDs (mainly frequency, power, and threshold voltage) will be used as a guide to predict the qualitative behavior of PGDs fabricated with the improved geometry of Fig. 1(a) and design the optimum epilayer to be grown for their later fabrication.

The distance between ohmic contacts of the simulated PGDs is $L = 0.5$–2.0 μm, with N_D in the range 0.2–10×10^{18} cm^{-3} and W between 150 and 400 nm. Since we are aiming to obtain GOs with the highest possible frequency, we will focus on the results obtained for $L = 0.5$ μm.

Simulations have been carried out by means of a semiclassical ensemble Monte Carlo tool self-consistently coupled with a 2-D Poisson solver [31], [38], [42], [43] in the time domain, for a total period of 0.1 ns with a time-step of $\Delta t = 0.2$ fs. The scattering mechanisms included in the simulations are intervalley, acoustic and optical (polar and nonpolar) phonons, piezoelectric, and ionized impurities. The conduction band of GaN is modeled by three nonparabolic spherical valleys (Γ_1, U, and Γ_3 valleys) by considering the Wurzite structure [44]. The lowest point of the conduction band is located at the Γ point (Γ_1-valley), 3.44 eV above the absolute maximum of the valence band, also located at the Γ point. The next minimum is located between the M and L points, leading to a valley (six equivalents) called the U-valley, at 2.2 eV from the minimum of the Γ_1-valley. The next minimum is located in the Γ_3-valley at 2.4 eV from the minimum of the Γ_1-valley. Other main parameters used in the simulation can be found in [26]. We are aware of recent experimental results [45] that show that the energy separation to the first satellite valley may be lower than the one considered in our model, about 0.9 eV (approximately the same as in previous reports such as [46], which obtain a value of 1.1 eV). We have not used such lower Γ_1–U valley separation in order to be consistent with our previous works, mainly taking into account the strong dispersion of the values of the parameters used for the Monte Carlo modeling of GaN (as described in the recent review by Lee *et al.* [47]). Moreover, the conclusions of our article would not be much modified, only lower values for the threshold voltages would be obtained. Therefore, the results presented in this work could be understood as "worst case" predictions.

The diodes will be simulated under two scenarios: 1) under the ideal condition of absence of surface charges at the top semiconductor-dielectric interface and 2) under the influence of surface charges, σ, whose local value will be calculated by using the self-consistent charge model (SCCM, explained detail in [48]), taking into account the carrier dynamics near the interface during the simulations.

III. Results and Discussion

Fig. 2(a) shows the I–V characteristics of the simulated PGDs for $L = 0.5$ μm, $W = 150$ nm, and N_D in the range 2–10×10^{18} cm^{-3} obtained with and without considering surface charges at the top interface. The inset shows the case $N_D = 5 \times 10^{18}$ cm^{-3} using the SCCM for $W = 150$–400 nm. As expected, the current level is practically proportional to N_D and W, and decreases just slightly when surface charges are accounted for in the simulations. Additionally, an NDR region is observed in all cases, enhanced as N_D and W increase. Such NDR is typically considered as evidence that GOs are taking place, but it is not a confirmation, since GOs can also appear without any noticeable feature in the I–V curve of the diodes [20], [49], [50] (and, on the other hand, the origin of the NDR can also be linked with experimental or physical factors, like self-heating or trap-related effects).

In order to show the presence or absence of GOs (and their main features when they emerge), the time-sequences of the simulated current corresponding to the I–V curves of Fig. 2(a)

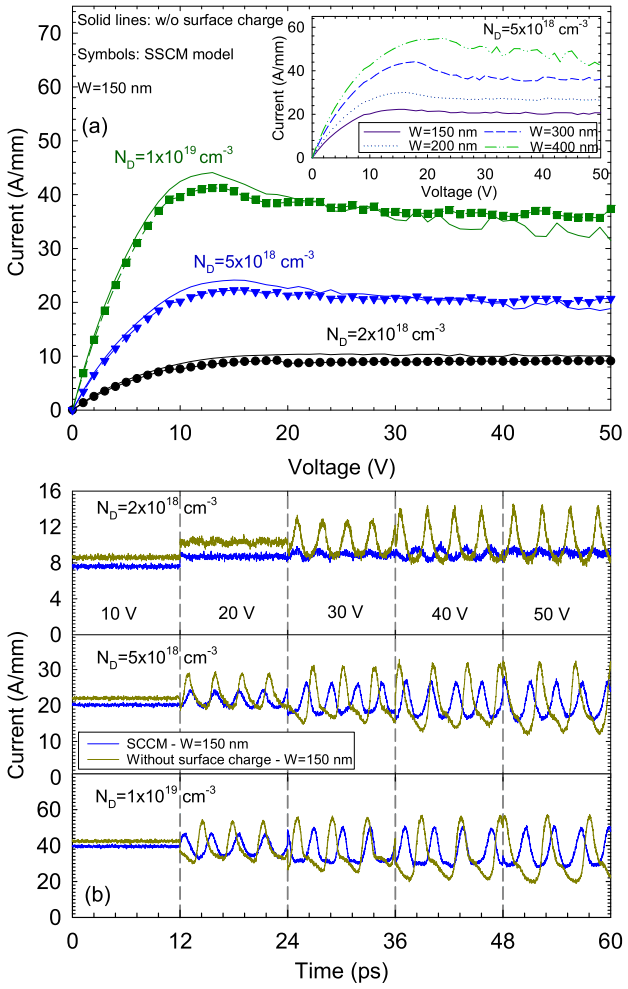

Fig. 2. (a) *I–V* curves in absence and presence (SCCM) of surface charge density for different doping levels and a width of the active region of 150 nm. The inset shows the *I–V* curves for $N_D = 5 \times 10^{18}$ cm^{-3} and *W* between 150 and 400 nm obtained with the SCCM. (b) Time-sequences of current density for applied biases in the 10–50 V range (step 10 V). In all cases $L = 0.5$ μm.

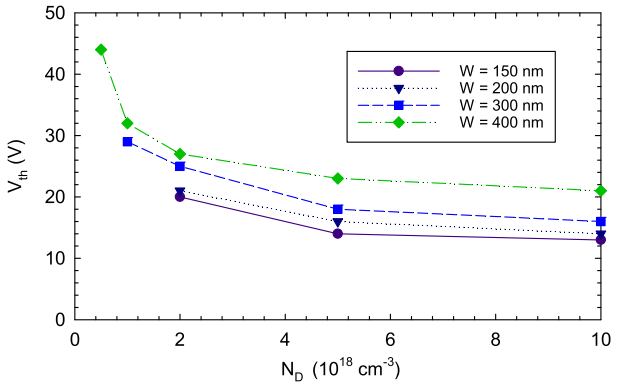

Fig. 3. V_{th} as a function of N_D for different values of *W* in the presence of surface charge (SCCM).

are shown in Fig. 2(b) for applied biases in the 10–50 V range (step 10 V). These results confirm that the onset of the GOs takes place in conjunction with the NDR in the *I–V* curves, with threshold voltages, V_{th}, in the 10–20 V range

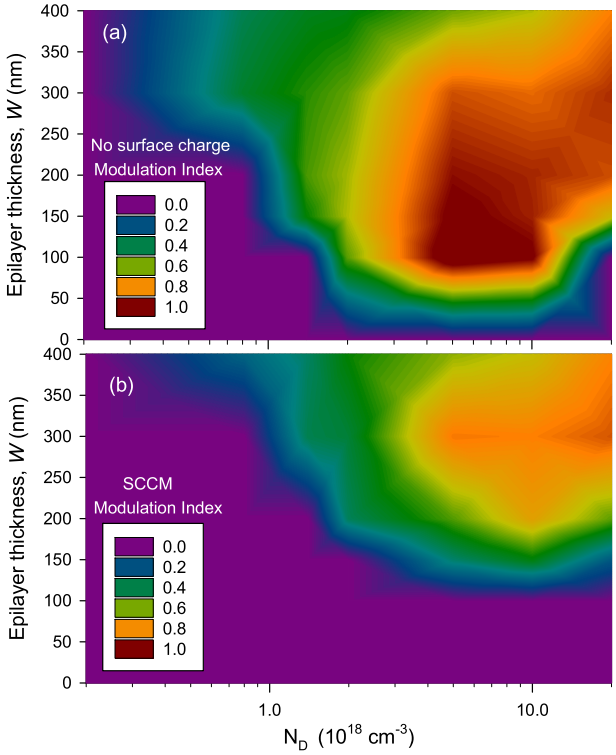

Fig. 4. Color map of the maximum of *MI*(*V*) versus N_D and *W* for $L = 0.5$ μm: (a) in absence of surface charge density and (b) including the presence of the surface charge (SCCM).

(and decreasing with the increase of N_D, as expected due to the enhanced strength of the electric field fluctuations). The value of V_{th}, see Fig. 3, decreases both with the increase of N_D and with the decrease of *W*, being below 15 V for thin epilayers ($W < 200$ nm) and values of N_D above 5×10^{18} cm^{-3}.

Although the effect of the surface charge on the average current is hardly noticeable, Fig. 2(a), it reduces the amplitude of the GOs and increases their frequency. However, the comparison between the oscillations obtained with the different values of N_D can only be done by means of a normalized indicator. For that sake, we define here a figure of merit characterizing the relative amplitude of the GOs (normalized by the saturation current, I_{sat}) for each bias, *V*: the modulation index, *MI*(*V*). We compute it as follows:

$$MI(V) = \frac{I_{max}(V) - I_{min}(V)}{I_{sat}} \quad (1)$$

being I_{max} and I_{min} the maximum and minimum values of the time-dependent diode current for each bias.

The values of the maximum of *MI*(*V*) (as a function of both N_D and *W*) are plotted as color maps in Fig. 4 in the absence and presence of surface charges (computed using the SCCM in the latter case). It clearly shows that, unexpectedly in view of its small influence on the *I–V* curves, the effect of the surface charge is critical, mainly for thin active layers ($W < 150$ nm) with low N_D.

If the surface charge is not considered, the optimal values for an efficient generation of GOs are found around $N_D = 5$–10×10^{18} cm^{-3} and $W = 100$–150 nm, where the *MI* reaches values near 1.0 (the amplitude of the current

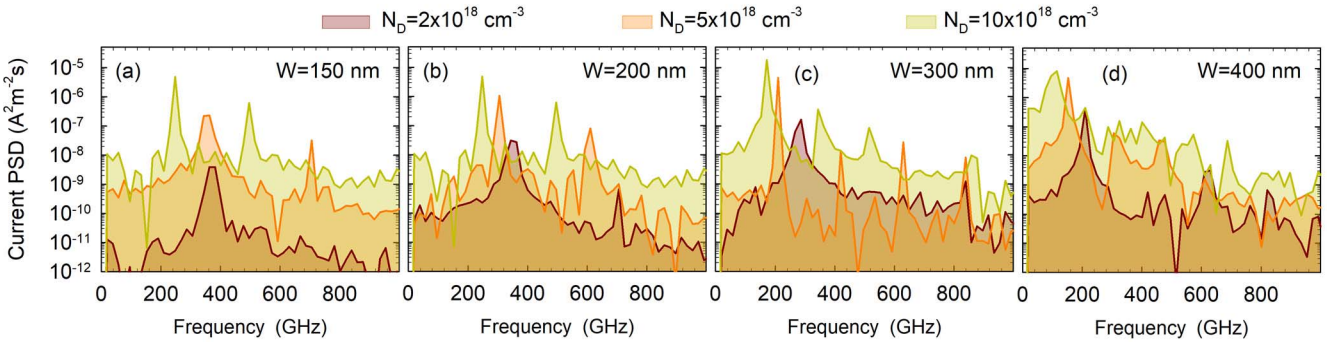

Fig. 5. Current PSD for (a) $W = 150$ nm, (b) 200 nm, (c) 300 nm, and (d) 400 nm for different N_D and $L = 0.5$ μm with an applied bias of 40 V.

oscillations is of the order of I_{sat}). However, if we analyze the realistic simulations using the SCCM, GOs are suppressed for $W \leq 100$ nm, even for high doping levels. This is due to the redistribution of the electric field originated by the presence of nonuniform surface charges. Surface charges at the top of the PGDs behave similarly (as a function of bias and position) to those at the sidewalls of the trenches in [31]. Electrons reach the top surface more easily when they are accelerated by the electric field, mainly at the anode side of the device, where they are trapped, thus making this region more resistive. This positive feedback makes the electric field to be concentrated in that region and thus exerts a strong influence on the onset of GOs.

In this case, the optimal values are found for higher values of N_D and W, around $N_D = 10^{19}$ cm^{-3} and $W = 300$ nm, where the *MI* reaches values around 0.8. But, under these ideal operation conditions of extremely high doping level and large epilayer thickness, the current level is so high that the extreme self-heating (for the applied voltages required for the onset of GOs), would lead to the catastrophic breakdown of the PGDs before oscillating. For example, for $N_D = 10^{19}$ cm^{-3} and $W = 300$ nm, the dc power is huge, above the 1.0 W/μm level at 20 V bias (current around 60 A/mm). This justifies the approach of using narrow channels (of around 300 nm) with shaped geometries in order to keep the self-heating at a reasonable intensity and avoid device burnout (the main problem faced when fabricating GaN vertical Gunn diodes [33]–[36]). For such designs, the current level would be around 2–10 mA per channel (depending on the doping level and active layer thickness), so that a 0.06–0.3 W dc power (at 30 V bias) would be dissipated, which is expected to be withstood by GaN.

Nevertheless, the technological process needed to fabricate such devices involves the etching of the active region in order to define the channels. The problem is that GaN is a hard material, so that a nonconventional process is needed, thus leading to the fact that the resolution of the lithography is degraded as the depth of the etching is increased. Therefore, it would be preferable not only to decrease the doping in order to decrease the current level, but also to keep the value of W below the 200 nm range, so that the lithographic process would be easier (with the additional advantage that the dissipated power will be further decreased).

For a better understanding of the features of the GOs, its power spectral density (PSD) is computed by Fourier transforming the long time-sequences of current obtained from the simulations. By using $2^{18} = 262\,144$ iterations with $\Delta t = 0.2$ fs, the frequency resolution of the current PSD is 19.07 GHz. The values of the PSD are plotted in Fig. 5 for W and N_D in the range 150–400 nm and 2–10 $\times$ 10^{18} cm^{-3}, respectively, at $V = 40$ V. Fig. 5 shows that the power of the fundamental harmonic of the GOs (and also the higher harmonics, when they appear) increases with N_D, as expected from a higher value of the dc current.

At low bias (not presented here) low amplitude plasma oscillations in the THz region are found for all devices [51]. When the applied voltage is increased above V_{th}, GOs take place in the 100–400 GHz range, evidenced by a huge increase of the PSD fundamental peak, whose frequency and amplitude (size of bubbles) is plotted in Fig. 6 as a function of the bias. The size of the bubbles has been adjusted in order to correctly compare the amplitudes obtained for the different doping levels. Taking as reference $N_D = 10^{19}$ cm^{-3}, the size of the bubbles has been multiplied by 4 and 25 for the cases of $N_D = 5 \times 10^{18}$ and 2×10^{18} cm^{-3}, respectively, since the dc current is expected to increase approximately by factors of 2 and 5 (and therefore, the PSD to be multiplied by $2^2 = 4$ and $5^2 = 25$). We can observe that the frequency of the GOs does not change much with the bias, but strongly depends on W and N_D, (found on a frequency range 100–400 GHz). Regarding the amplitude of the oscillations, it is also fairly constant once the GOs are stable, when the bias is well above V_{th}.

When the thickness of the doped layer is reduced from $W = 400$–150 nm, the frequency of the GOs increases significantly, regardless of N_D (by a factor of 2 for the lowest N_D and even 3 for the highest), but with much lower amplitude. This means that the formation of the Gunn domain is progressively shifted near to the anode region as W decreases, thus reducing the transit time of the domain, but, on the other hand, leading to a noncomplete maturation of the domain, thus reducing the amplitude of the GOs. This is due to a stronger concentration of the electric field in the anode region, which is compatible with the observed decrease of the value of V_{th}, see Fig. 3, from $\sim$24 V for $W = 400$ nm to $\sim$16 V for 150 nm in the case of $N_D = 5 \times 10^{18}$ cm^{-3}.

Therefore, the choice of W is a tradeoff between high frequency and high power, but it cannot be chosen freely, since it is limited by the technological process used to define the shape of the channels as shown in Fig. 1(a). Also, a thick

doped layer leads to stronger self-heating effects, mainly for high values of N_D (as found in [41] for $W = 400$ nm and $N_D = 2.4 \times 10^{18}$ cm^{-3}). Therefore, a low value of W, below 200 nm, would be preferable, in order not only to simplify the lithography but also to reduce the thermal risks, also with the benefit that the oscillation frequency is increased. The (important) price to pay is the lower efficiency of the GOs.

Regarding the doping level, $N_D = 5 \times 10^{18}$ cm^{-3} seems to be the optimum value, since a further increase of N_D does not produce an increase of the relative amplitude of the GOs, as it was also observed in Fig. 4 when representing the values of the *MI*. Therefore, a further increase of N_D should be avoided, since it magnifies the self-heating effects and decreases the frequency of the GOs.

The simulations of longer PGDs (with $L = 1.0$ and 2.0 μm) exhibit qualitatively the same dependencies on W and N_D observed before for $L = 0.5$ μm. However, as expected, GOs start at a higher threshold voltage and are of lower frequency (both roughly scaling with the length), while the amplitude is slightly higher. We have also found that GOs could be obtained with a narrower active layer of $W = 100$ nm, but with scarce ac power.

We will focus now on epilayers with $W = 150$ nm, at the lower limit of the thickness for which GOs are observed, and therefore, with the highest frequency, which is the aim of our optimization process. Fig. 7 shows the color map of the current PSD of the GOs as a function of the applied bias at 300 and 600 K, in order to show the effect that the extreme self-heating conditions will have on the GOs. The figure shows that even at 600 K, near the limit of the operating conditions that GaN devices can withstand, GOs are not significantly degraded (even if the frequency of the oscillation is slightly lower and its spectral purity is poorer). For example, for $N_D = 2 \times 10^{18}$ cm^{-3} [Fig. 7(a) and (d)] only the fundamental harmonic of the GOs is observed, with a frequency in the 360–380 GHz range at 300 K, which decreases to 340–360 GHz for 600 K, and, in this case, surprisingly, the amplitude of the GOs increases. This happens because the value of the negative differential mobility in the v–E curve of GaN does not depend much on the lattice temperature, only an increase of the peak electric field is observed when heating the material.

This is a very significant result because, even if the definition of narrow channels in shaped PGDs, as shown in Fig. 1(a), would mitigate the self-heating effects, GOs would not be terminated by a significant temperature increase, which would inevitably appear when using such highly doped active layers. We also want to stress that the efficiency of GOs would be improved in such shaped PGDs, but the epilayer optimization rules previously obtained would still be applicable.

For larger N_D, the fundamental oscillation frequency decreases to ~350 and ~320 GHz, for 5×10^{18} and 10×10^{18} cm^{-3}, respectively, and a still powerful second harmonic arises, reaching frequencies in the 600–700 GHz range (even if at 600 K, the current PSD for the second harmonic is slightly degraded). It is also remarkable that even the third harmonic appears clearly, even at 600 K with $N_D = 5 \times 10^{18}$ cm^{-3}, meaning that ac power could be extracted from a GaN PGD at frequencies above 1.0 THz by an appropriate filtering circuit. Even if this is also a remarkable observation, practical problems such as crosstalk capacitances and substrate and circuit losses may hinder the power generation at such high frequencies, which should be analyzed not only from the point of view of epilayer and device optimization but also from layout and circuit design.

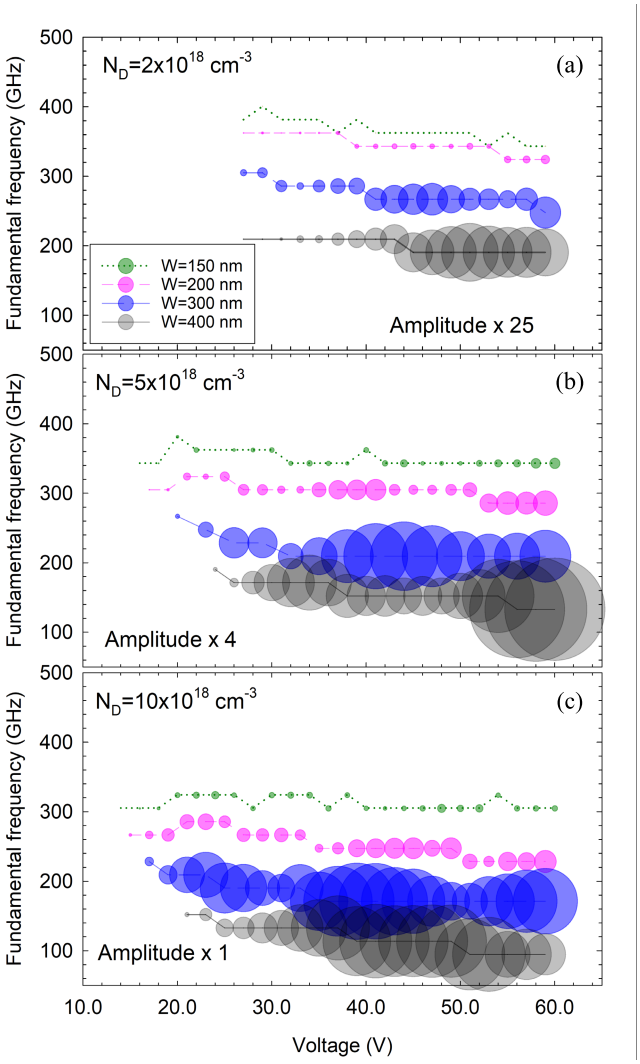

Fig. 6. Frequency of the fundamental harmonic of the GOs versus bias for (a) $N_D = 2 \times 10^{18}$ cm^{-3}, (b) 5×10^{18} cm^{-3}, and (c) 10×10^{18} cm^{-3} and different values of W and $L = 0.5$ μm. The amplitude of the current PSD at the frequency of the fundamental harmonic is represented by the size of the bubbles, which has been multiplied by 25 and 4 in (a) and (b), respectively, in order to well compare the efficiency of the oscillations for different values of N_D.

IV. Conclusion

By means of Monte Carlo simulations of GaN PGDs based on a doped active layer, we have provided the optimum epilayer design for achieving ultrahigh-frequency GOs with the best possible efficiency. Apart from simulation results, practical constraints for the fabrication and continuous-wave operation of the devices have been considered. In particular, too thick layers should be avoided, since they hinder the lithographic process and lead to an excessive power dissipation

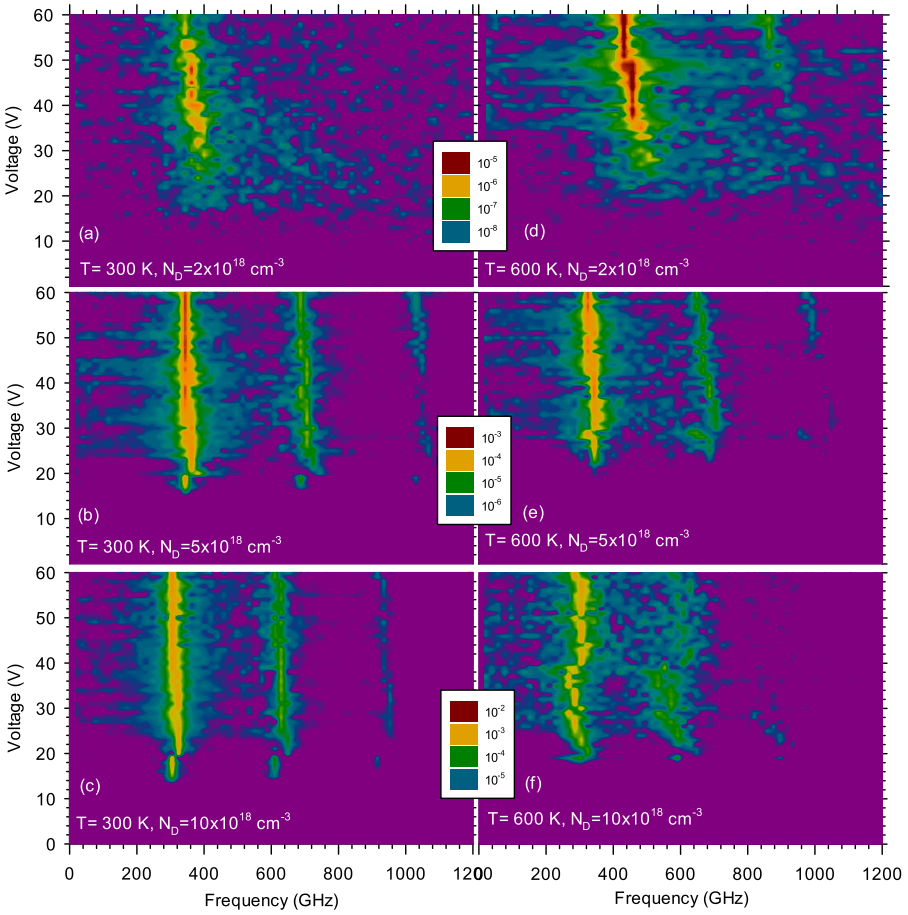

Fig. 7. Color maps of the current PSD versus applied voltage for $N_D = 2 \times 10^{18}$, 5×10^{18}, and 10×10^{18} cm^{-3} and $W = 150$ nm, computed at lattice temperatures of (a)–(c) 300 K and (d)–(f) 600 K. The units of the PSD are the same as in Fig. 5, A^{2}m^{-2}s (note that color scale changes with N_D).

and catastrophic self-heating. As a result, we propose the use of active layers with $W = 150$ nm and $N_D = 5 \times 10^{18}$ cm^{-3}. With such an epilayer, PGDs with $L = 0.5$ μm would exhibit GOs with a fundamental frequency around 350 GHz and a significant ac power. Even if it is not possible to directly estimate the RF output power from the simulations presented in this work (no load is connected to the Gunn diode), we expect the GaN PGDs studied here to provide similar efficiencies to those of Gunn diodes based on vertical n^+nn^+ structures and AlGaN/GaN-based nanochannels for frequencies around 250–350 GHz (see [30], [32], [38]), in the 0.1%–1% range. Assuming a 0.5% efficiency, the output RF power that would be ideally generated by the fundamental harmonic of the GaN PGDs with the optimum epilayers design is around 4.0 mW/μm at 350 GHz (corresponding to 1.2 mW for a single 300 nm wide channel, with $P_{dc} \sim 240$ mW, which may be further parallelized for obtaining higher power levels with the only constraint of enhanced self-heating problems).

Higher doping levels could also be implemented if a larger power is needed, but the oscillation frequency would slightly decrease, and, again, more stringent heating dissipation techniques should be used (use of heat sinking mounting, air-cooling, or even cryogenic cooling systems). Therefore, the optimum epilayer design would correspond to the lowest doping allowing for the onset of the GOs, which provides not only limited self-heating, but also higher oscillation frequencies. In any case, simulations show that GOs are still present when GaN PGDs operate at high temperatures, so that thermal management strategies should be developed.

The optimization of the epilayer presented here is the first step in the design of shaped channel PGDs, whose optimum geometry as a function of the target frequency and generated power will be analyzed in future works.

REFERENCES

[1] M. Tonouchi, "Cutting-edge terahertz technology," *Nature Photon.*, vol. 1, pp. 97–105, Oct. 2007.
[2] P. H. Siegel, "Terahertz technology in biology and medicine," in *IEEE MTT-S Int. Microw. Symp. Dig.*, Jun. 2004, pp. 1575–1578.
[3] M. A. Belkin *et al.*, "Terahertz quantum-cascade-laser source based on intracavity difference-frequency generation," *Nature Photon.*, vol. 1, no. 5, pp. 288–292, 2007.
[4] J. V. Siles and J. Grajal, "Physics-based design and optimization of Schottky diode frequency multipliers for terahertz applications," *IEEE Trans. Microw. Theory Techn.*, vol. 58, no. 7, pp. 1933–1942, Jun. 2010.
[5] H. Eisele, "State of the art and future of electronic sources at terahertz frequencies," *Electron. Lett.*, vol. 46, no. 26, p. S8, 2010.
[6] I. Mehdi, J. V. Siles, C. Lee, and E. Schlecht, "THz diode technology: Status, prospects, and applications," *Proc. IEEE*, vol. 105, no. 6, pp. 990–1007, Jun. 2017.
[7] D. Pukala *et al.*, "Submillimeter-wave InP MMIC amplifiers from 300–345 GHz," *IEEE Microw. Wireless Compon. Lett.*, vol. 18, no. 1, pp. 3–61, Jan. 2008.

[8] V. Radisic *et al.*, "A 10-mW submillimeter-wave solid-state power-amplifier module," *IEEE Trans. Microw. Theory Techn.*, vol. 58, no. 7, pp. 1903–1909, Jun. 2010.

[9] N. Orihashi, S. Suzuki, and M. Asada, "One THz harmonic oscillation of resonant tunneling diodes," *Appl. Phys. Lett.*, vol. 87, no. 23, Dec. 2005, Art. no. 233501.

[10] S. Suzuki, A. Teranishi, K. Hinata, M. Asada, H. Sugiyama, and H. Yokoyama, "Fundamental oscillation up TO 831 GHz in GaInAs/AlAs resonant tunneling diode," in *Proc. IEEE Int. Conf. Indium Phosph. Rel. Mater.*, May 2009, pp. 192–195,

[11] K. Kobayashi, S. Suzuki, F. Han, H. Tanaka, H. Fujikata, and M. Asada, "Analysis of a high-power resonant-tunneling-diode terahertz oscillator integrated with a rectangular cavity resonator," *Jpn. J. Appl. Phys.*, vol. 59, no. 5, May 2020, Art. no. 050907.

[12] M. Ino, T. Ishibashi, and M. Ohmori, "CW oscillation with p^+-p-n^+ silicon IMPATT diodes in 200 GHz and 300 GHz bands," *Electron. Lett.*, vol. 12, no. 6, pp. 148–149, Mar. 1976.

[13] K. Chang, F. Thrower, and G. M. Hayashibara, "Millimeter-wave silicon IMPATT sources and combiners for the 110-260 GHz range," in *IEEE MTT-S Int. Microw. Symp. Dig.*, Jun. 1981, pp. 344–346.

[14] H. Eisele, A. Rydberg, and G. I. Haddad, "Recent advances in the performance of InP Gunn devices and GaAs TUNNETT diodes for the 100–300-GHz frequency range and above," *IEEE Trans. Microw. Theory Techn.*, vol. 48, no. 4, pp. 626–631, Apr. 2000.

[15] H. Eisele, "355 GHz oscillator with GaAs TUNNETT diode," *Electron Lett.*, vol. 41, no. 6, pp. 329–331, Mar. 2005.

[16] J. Nishizawa, P. Płotka, T. Kurabayashi, and H. Makabe, "706-GHz GaAs CW fundamental-mode TUNNETT diodes fabricated with molecular layer epitaxy," *Phys. Status Solidi C*, vol. 5, no. 9, pp. 2802–2804, Jul. 2008.

[17] J. B. Gunn, "Microwave oscillations of current in III–V semiconductors," *Solid State Commun.*, vol. 1, no. 4, pp. 88–91, Sep. 1963.

[18] H. Kroemer, "Theory of the Gunn effect," *Proc. IEEE*, vol. 52, no. 12, p. 1736, Dec. 1964, doi: 10.1109/PROC.1964.3476.

[19] M. MI *et al.*, "An AlGaAs/GaAs-based planar Gunn diode oscillator with a fundamental frequency operation of 120 GHz," *Microw. Opt. Technol. Lett.* vol. 56, no. 10, pp. 2449–2451, 2014.

[20] A. Khalid *et al.*, "Terahertz oscillations in an $In_{0.53}Ga_{0.47}As$ submicron planar Gunn diode," *J. Appl. Phys.*, vol. 115, no. 11, Mar. 2014, Art. no. 114502.

[21] L. Dunleavy, C. Baylis, W. Curtice, and R. Connick, "Modeling GaN: Powerful but challenging," *IEEE Microw. Mag.*, vol. 11, no. 6, pp. 82–96, Oct. 2010.

[22] L. Shen *et al.*, "AlGaN/AlN/GaN high-power microwave HEMT," *IEEE Electron Device Lett.*, vol. 22, no. 10, pp. 457–459, Oct. 2001.

[23] J.-Y. Duboz, "GaN as seen by the industry," *Comp. Rendus l'Académie Sci. Phys.*, vol. 1, no. 1, pp. 71–80, Mar. 2000.

[24] H. Amano *et al.*, "The 2018 GaN power electronics roadmap," *J. Phys. D, Appl. Phys.*, vol. 51, no. 16, Mar. 2018, Art. no. 163001.

[25] L. Yang, S. Long, X. Guo, and Y. Hao, "A comparative investigation on sub-micrometer InN and GaN Gunn diodes working at terahertz frequency," *J. Appl. Phys.*, vol. 111, no. 10, May 2012, Art. no. 104514.

[26] S. García, S. Pérez, I. Í˜ñiguez-de-la-Torre, J. Mateos, and T. González, "Comparative Monte Carlo analysis of InP-and GaN-based Gunn diodes," *J. Appl. Phys.*, vol. 115, no. 4, Jan. 2014, Art. no. 044510.

[27] V. Gruzinskis, P. Shiktorov, E. Starikov, and J. H. Zhao, "Comparative study of 200-300 GHz microwave power generation in GaN TEDs by the Monte Carlo technique," *Semicond. Sci. Technol.*, vol. 16, no. 9, pp. 798–805, Sep. 2001.

[28] C. Sevik and C. Bulutay, "Gunn oscillations in GaN channels," *Semicond. Sci. Technol.*, vol. 19, no. 4, pp. S188–S190, Apr. 2004.

[29] R. P. Joshi, V. Sridhara, P. Shah, and R. D. Del Rosario, "Monte Carlo analysis of GaN-based Gunn oscillators for microwave power generation," *J. Appl. Phys.*, vol. 93, no. 8, pp. 4836–4842, 2003.

[30] S. García, I. Ìñiguez-de-la-Torre, S. Pérez, J. Mateos, and T. González, "Numerical study of sub-millimeter Gunn oscillations in InP and GaN vertical diodes: Dependence on bias, doping, and length," *J. Appl. Phys.*, vol. 114, no. 7, Aug. 2013, Art. no. 074503.

[31] J.-F. Millithaler *et al.*, "Optimized V-shape design of GaN nanodiodes for the generation of Gunn oscillations," *Appl. Phys. Lett.*, vol. 104, no. 7, Feb. 2014, Art. no. 073509.

[32] S. Garcia, B. G. Vasallo, J. Mateos, and T. Gonzalez, "Time-domain Monte Carlo simulations of resonant-circuit operation of GaN Gunn diodes," in *Proc. Spanish Conf. Electron Devices*, Feb. 2013, pp. 79–82.

[33] O. Yilmazoglu, K. Mutamba, D. Pavlidis, and T. Karaduman, "Measured negative differential resistivity for GaN Gunn diodes on GaN substrate," *Electron. Letters.*, vol. 43, no. 8, pp. 480–482, 2007.

[34] O. Yilmazoglu, K. Mutamba, D. Pavlidis, and T. Karaduman, "First observation of bias oscillations in GaN Gunn diodes on GaN substrate," *IEEE Trans. Electron Devices*, vol. 55, no. 6, pp. 1563–1567, May 2008.

[35] A. S. Hajo, O. Yilmazoglu, B. Samodi, A. Dadgar, F. Kuppers, and T. Kussorow, "A new approach to achieve Gunn effect for GaN based THz sources with high power," in *Proc. 44th Int. Conf. Infr., Millim., THz Waves (IRMMW-THz)*, Sep. 2019, pp. 1–2.

[36] A. S. Hajo, O. Yilmazoglu, A. Dadgar, F. Küppers, and T. Kusserow, "Reliable GaN-based THz Gunn diodes with side-contact and field-plate technologies," *IEEE Access*, vol. 8, pp. 84116–84122, 2020.

[37] M. Takeuchi, A. Higashisaka, and K. Sekido, "GaAs planar Gunn diodes for DC-biased operation," *IEEE Trans. Electron Devices*, vol. ED-19, no. 1, pp. 125–127, Jan. 1972.

[38] B. G. Vasallo *et al.*, "Monte Carlo study of the operation of GaN planar nanodiodes as sub-THz emitters in resonant circuits," *Semicond. Sci. Technol.*, vol. 29, no. 11, Nov. 2014, Art. no. 115032.

[39] J. Mateos *et al.*, "Design and fabrication of planar Gunn nanodiodes based on doped GaN," in *Proc. IEEE Asia–Pacific Microw. Conf. (APMC)*, Dec. 2019, pp. 971–973.

[40] M. Agrawal *et al.*, "GaN-based SSD structure for THz applications," in *Proc. IEEE Asia–Pacific Microw. Conf. (APMC)*, Dec. 2019, pp. 213–215.

[41] S. García-Sánchez *et al.*, "Non-linear thermal resistance model for the simulation of high power GaN-based devices," *Semicond. Sci. Technol.*, vol. 36, no. 5, May 2021, Art. no. 055002.

[42] C. Jacoboni and P. Lugli, *The Monte Carlo Method for Semiconductor Device Simulation*. New York, NY, USA: Springer-Verlag, 1989.

[43] A. Íñiguez-de-la-Torre *et al.*, "Searching for THz Gunn oscillations in GaN planar nanodiodes," *J. Appl. Phys.*, vol. 111, no. 11, p. 113705, 2012.

[44] O. Madelung, *Semiconductors: Data Handbook*. Berlin, Germany: Springer, 2004.

[45] M. Piccardo *et al.*, "Determination of the first satellite valley energy in the conduction band of Wurtzite GaN by near-band-gap photoemission spectroscopy," *Phys. Rev. B, Condens. Matter*, vol. 89, no. 23, Jun. 2014, Art. no. 235124.

[46] O. Yilmazoglu, D. Pavlidis, H. L. Hartnagel, A. Evtukh, V. Litovchenko, and N. Semenenko, "Evidence of satellite valley position in GaN by photoexcited field emission spectroscopy," *J. Appl. Phys.*, vol. 103, no. 11, Jun. 2008, Art. no. 114511.

[47] W. Z. Lee, D. S. Ong, K. Y. Choo, O. Yilmazoglu, and H. L. Hartnagel, "Monte Carlo evaluation of GaN THz Gunn diodes," *Semicond. Sci. Technol.*, vol. 36, no. 12, Dec. 2021, Art. no. 125009.

[48] I. Iñiguez-De-La-Torre *et al.*, "Influence of the surface charge on the operation of ballistic T-branch junctions: A self-consistent model for Monte Carlo simulations," *Semicond. Sci. Technol.*, vol. 22, no. 6, p. 663, 2007.

[49] A. Khalid *et al.*, "$In_{0.53}Ga_{0.47}As$ planar Gunn diodes operating at a fundamental frequency of 164 GHz," *IEEE Electron Device Lett.*, vol. 34, no. 1, pp. 39–41, Nov. 2013.

[50] M. I. Maricar, A. Khalid, D. R. S. Cumming, and C. H. Oxley, "Extraction of second harmonic from an InP based planar Gunn diode using diamond resonator for milli-metric wave frequencies," *Solid-State Electron.*, vol. 116, pp. 104–106, Feb. 2016.

[51] L. Reggiani, P. Golinelli, E. Faucher, L. Varani, T. González, D. Pardo *Proceedings of the 13th International Conference of Noise in Physical Systems and 1/f Fluctuations*, V. Bareikis and R. Katilius, Eds. Singapore: World Scientific, 1995.